We are IntechOpen,
the world's leading publisher of
Open Access books
Built by scientists, for scientists

6,900
Open access books available

185,000
International authors and editors

200M
Downloads

Our authors are among the

154
Countries delivered to

TOP 1%
most cited scientists

12.2%
Contributors from top 500 universities

CLARIVATE ANALYTICS
BOOK CITATION INDEX
INDEXED

WEB OF SCIENCE™

Selection of our books indexed in the Book Citation Index
in Web of Science™ Core Collection (BKCI)

Interested in publishing with us?
Contact book.department@intechopen.com

Propagation in Lossy Rectangular Waveguides

Kim Ho Yeap[1], Choy Yoong Tham[2],
Ghassan Yassin[3] and Kee Choon Yeong[1]
[1]Tunku Abdul Rahman University
[2]Wawasan Open University
[3]University of Oxford
[1,2]Malaysia
[3]United Kingdom

1. Introduction

In millimeter and submillimeter radio astronomy, waveguide heterodyne receivers are often used in signal mixing. Wave guiding structures such as circular and rectangular waveguides are widely used in such receiver systems to direct and couple extraterrestrial signals at millimeter and submillimeter wavelengths to a mixer circuit (Carter et al., 2004; Boifot et al., 1990; Withington et al., 2003).

To illustrate in detail the applications of waveguides in receiver systems, a functional block diagram of a typical heterodyne receiver in radio telescopes is shown in Fig. 1 (Chattopadhyay et al., 2002). The electromagnetic signal (RF signal) from the antenna is directed down to the front end of the receiver system via mirrors and beam waveguides (Paine et al., 1994). At the front end of the receiver system, such as the sideband separating receiver designed for the ALMA band 7 cartridge (Vassilev and Belitsky, 2001a; Vassilev and Belitsky, 2001b; Vassilev et al., 2004), the RF signal is channelled from the aperture of the horn through a circular and subsequently a rectangular waveguide, before being coupled to the mixer. In the mixer circuit, a local oscillator (LO) signal which is generally of lower frequency is then mixed with the RF signal, to down convert the RF signal to a lower intermediate frequency (IF) signal. Here, a superconductor-insulator-superconductor (SIS) heterodyne mixer is commonly implemented for the process of down conversion. At the back end of the system, the IF signal goes through multiple stages of amplification and is, eventually, fed to a data analysis system such as an acousto-optic spectrometer. The data analysis system will then be able to perform Fourier transformation and record spectral information about the input signal.

The front-end receiver noise temperature T_R is determined by a number of factors. These include the mixer noise temperature T_M, the conversion loss C_{Loss}, the noise temperature of the first IF amplifier T_{IF}, and the coupling efficiency between the IF port of the junction and the input port of the first IF amplifier η_{IF}. A comparison of the performance of different SIS waveguide receivers is listed in Table 1 (Walker et al., 1992). It can be seen that the value of T_R for the 230 GHz system is a factor of 3 to 4 less than that achieved with the 492 GHz system. The decrease in system performance at 492 GHz is due to the increase of C_{Loss} and T_M by a factor of approximately 3.
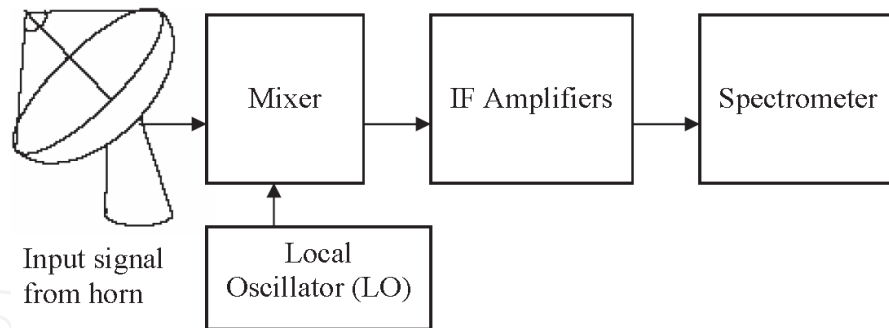
Fig. 1. Block diagram of a heterodyne receiver.

SIS Junction	Nb	Pb	Nb
Center Frequency (GHz)	230	345	492
T_R (K)	48	159	176
T_M (K)	34	129	123
C_{Loss} (dB)	3.1	8.1	8.9
T_{IF} (K)	7.0	4.2	6.8

Table 1. Comparison of SIS receiver performance.

Since the input power level of the weak millimeter and submillimeter signals is quite small – i.e. of the order of 10^{-18} to 10^{-20} W (Shankar, 1986), it is therefore of primary importance to minimize the conversion loss C_{Loss} of the mixer circuit. One way of doing so, is to ensure that the energy of the LO and, in particular, the RF signals is channelled and coupled from the waveguides to the mixer circuit in a highly efficient manner. It is simply too time consuming and too expensive to develop wave guiding structures in a receiver system on a trial-and-error basis. To minimize the loss of the propagating signals, the availability of an accurate and easy-to-use mathematical model to compute the loss of such signals in wave guiding structures is, of course, central to the development of receiver circuits.

2. Related work

Analysis of the propagation of wave in circular cylindrical waveguides has already been widely performed (Glaser, 1969; Yassin et al., 2003; Claricoats, 1960a; Claricoats, 1960b; Chou and Lee, 1988). The analyses by these authors are all based on the rigorous method formulated by Stratton (1941). In Stratton's formulation, the fields at the wall surface are made continuous into the wall material. Assumption made on the field decaying inside the wall material yields relations which allow the propagation constant to be determined. Due to the difficulty in matching the boundary conditions in Cartesian coordinates, this approach, however fails to be implemented in the case of rectangular waveguides. A similar rigorous technique to study the attenuation of rectangular waveguides is not available hitherto.
The perturbation power-loss method has been commonly used in analyzing wave attenuation in lossy (Stratton, 1941; Seida, 2003; Collin 1991; Cheng, 1989) and superconducting (Winters and Rose, 1991; Ma, 1998; Wang et al., 1994; Yalamanchili et al., 1995) rectangular waveguides; respectively. This is partly due to its ability to produce simple analytical solution, and also partly because it gives reasonably accurate result at frequencies f well above its cutoff frequency f_c. In this method, the field expressions are derived by assuming that the walls to be of infinite conductivity. This allows the solution to

be separated into pure Transverse Electric (TE) and Transverse Magnetic (TM) modes. For a waveguide with finite conductivity, however, a superposition of both TE and TM modes is necessary to satisfy the boundary conditions (Stratton, 1941; Yassin et al., 2003). This is because, unlike those of the lossless case, the modes in a lossy waveguide are no longer mutually orthogonal to each other (Collin, 1991). To calculate the attenuation, ohmic losses are assumed due to small field penetration into the conductor surface. Results however show that this method fails near cutoff, as the attenuation obtained diverges to infinity when the signal frequency f approaches the cutoff f_c. Clearly, it is more realistic to expect losses to be high but finite rather than diverging to infinity. The inaccuracy in the power-loss method at cutoff is due to the fact that the field equations are assumed to be identical to those of a lossless waveguide. Since a lossless waveguide behaves exactly like an ideal high pass filter, signals cease to propagate at f below f_c.

It can be seen that the assumption of lossless fields fail to give an insight or deeper understanding on the mechanism of the propagation of wave in practical lossy waveguides. Moreover, at very high frequency – especially that approaches the millimeter and submillimeter wavelengths – the loss tangent of the conducting wall decreases. Therefore, such assumption turns out to be inaccurate at very high frequency. Although Stratton (1941) has developed a truly fundamental approach to analyze waveguides, his approach is only restricted to the case of circular waveguides and could not be applied to rectangular waveguides. The workhorse of this chapter is, therefore, to develop a novel and accurate formulation – i.e. one that does not assume lossless boundary conditions – to investigate the loss of waves in rectangular waveguides. In particular, the new method shall be found more accurate and useful for waveguides operating at very high frequencies, such as those in the millimeter and submillimeter wavelengths. In Yeap et al. (2009), a simple method to compute the loss of waves in rectangular waveguides has been developed. However, the drawback of the method is that different sets of characteristic equation are required to solve for the propagation constants of different modes. Here, the method proposed in Yeap et al. (2009) shall be developed further so that the loss of different modes can be conveniently computed using only a single set of equation. For convenience purpose, the new method shall be referred to as the boundary-matching method in the subsequent sections.
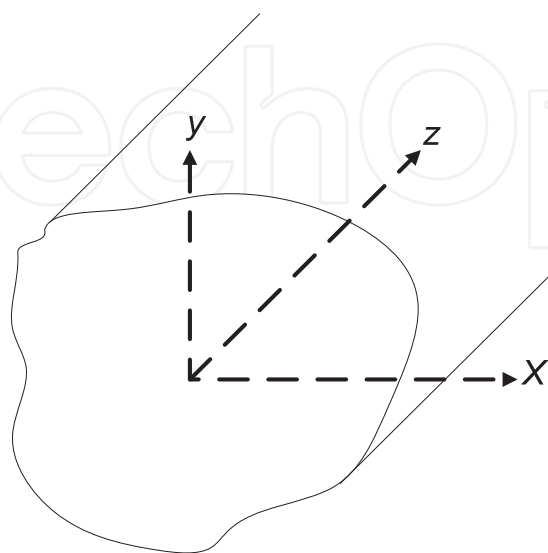

Fig. 2. A waveguide with arbitrary geometry.

3. General wave behaviours along uniform guiding structures

As depicted in Fig. 2, a time harmonic field propagating in the z direction of a uniform guiding structure with arbitrary geometry can be expressed as a combination of elementary waves having a general functional form (Cheng, 1989)

$$\psi = \psi^0 \left(x, y\right) \exp[j(\omega t + k_z z)] \tag{1}$$

where $\psi^0(x, y)$ is a two dimensional vector phasor that depends only on the cross-sectional coordinates, $\omega = 2\pi f$ the angular frequency, and k_z is the propagation constant.

Hence, in using phasor representation in equations relating field quantities, the partial derivatives with respect to t and z may be replaced by products with $j\omega$ and jk_z, respectively; the common factor $\exp[j(\omega t + k_z z)]$ can be dropped. Here, the propagation constant k_z is a complex variable, which consists of a phase constant β_z and an attenuation constant a_z

$$k_z = \beta_z - j\alpha_z \tag{2}$$

The field intensities in a charge-free dielectric region (such as free-space), satisfy the following homogeneous vector Helmholtz's equation

$$\nabla^2 \psi_z + (k^2 - k_z{}^2)\psi_z = 0 \tag{3}$$

where ψ_z is the longitudinal component of $\boldsymbol{\psi}$, ∇^2 is the Laplacian operator for the transverse coordinates, and k is the wavenumber in the material. For waves propagating in a hollow waveguide, $k = k_0$, the wavenumber in free-space.

It is convenient to classify propagating waves into three types, in correspond to the existence of the longitudinal electric field E_z or longitudinal magnetic H_z field:

1. Transverse electromagnetic (TEM) waves. A TEM wave consists of neither electric fields nor magnetic fields in the longitudinal direction.
2. Transverse magnetic (TM) waves. A TM wave consists of a nonzero electric field but zero magnetic field in the longitudinal direction.
3. Transverse electric (TE) waves. A TE wave consists of a zero electric field but nonzero magnetic field in the longitudinal direction.

Single-conductor waveguides, such as a hollow (or dielectric-filled) circular and rectangular waveguide, cannot support TEM waves. This is because according to Ampere's circuital law, the line integral of a magnetic field around any closed loop in a transverse plane must equal the sum of the longitudinal conduction and displacement currents through the loop. However, since a single-conductor waveguide does not have an inner conductor and that the longitudinal electric field is zero, there are no longitudinal conduction and displacement current. Hence, transverse magnetic field of a TEM mode cannot propagate in the waveguide (Cheng, 1989).

4. Fields in cartesian coordinates

For waves propagating in a rectangular waveguide, such as that shown in Fig. 3, Helmholtz's equation in (3) can be expanded in Cartesian coordinates to give

$$\frac{\partial^2 \psi_z}{\partial x^2} + \frac{\partial^2 \psi_z}{\partial y^2} + \left(k^2 - k_z^2\right)\psi_z = 0 \tag{4}$$

By applying the method of separation of variables, ψ_z can be expressed as

$$\psi_z = X(x)Y(y) \tag{5}$$

Equation (4) can thus be separated into two sets of second order differential equations, as shown below (Cheng, 1989)

$$\frac{d^2 X(x)}{dx^2} + k_x^2 X(x) = 0 \tag{6}$$

$$\frac{d^2 Y(y)}{dy^2} + k_y^2 Y(y) = 0 \tag{7}$$

where k_x and k_y are the transverse wavenumbers in the x and y directions, respectively. The longitudinal fields can be obtained by solving (6) and (7) based on a set of boundary conditions and substituting the solutions into (5).
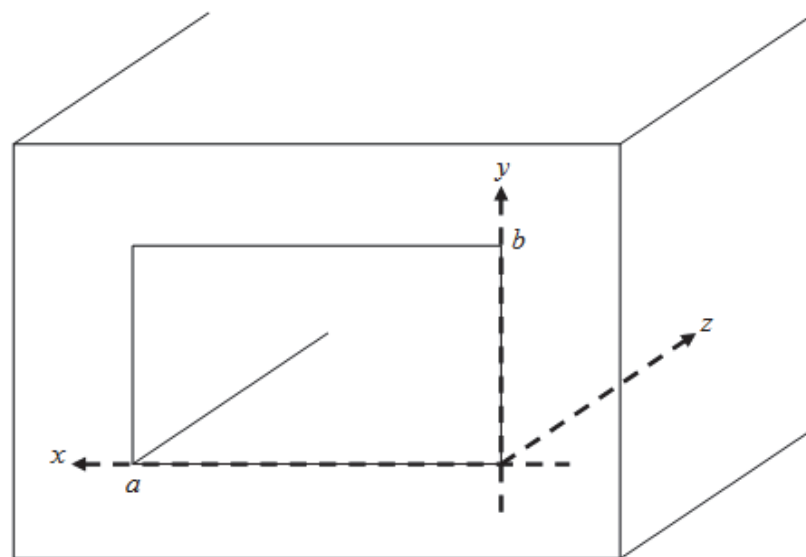

Fig. 3. The cross section of a rectangular waveguide.

The transverse field components can be derived by substituting the longitudinal field components into Maxwell's source free curl equations

$$\nabla \times E = \text{-}j\omega\mu H \tag{8}$$

$$\nabla \times H = j\omega\varepsilon E \tag{9}$$

where ε and μ are the permittivity and permeability of the material, respectively. Expressing the transverse field components in term of the longitudinal field components E_z and H_z, the following equations can be obtained (Cheng, 1989)

$$H_x = \frac{-j}{k_x^2 + k_y^2}\left(k_z \frac{dH_z}{dx} - \omega\varepsilon \frac{dE_z}{dy} \right) \tag{10}$$

$$H_y = \frac{-j}{k_x^2 + k_y^2}\left(k_z \frac{dH_z}{dy} + \omega\varepsilon \frac{dE_z}{dx} \right) \tag{11}$$

$$E_x = \frac{-j}{k_x^2 + k_y^2}\left(k_z \frac{dE_z}{dx} + \omega\mu \frac{dH_z}{dy} \right) \tag{12}$$

$$E_y = \frac{-j}{k_x^2 + k_y^2}\left(k_z \frac{dE_z}{dy} - \omega\mu \frac{dH_z}{dx} \right) \tag{13}$$

5. Review of the power-loss method

In the subsequent sections, analysis and comparison between the perturbation power-loss method and the new boundary matching method shall be performed. Hence, in order to present a complete scheme, the derivation of the conventional power-loss method is briefly outlined in this section.

The attenuation of electromagnetic waves in waveguides can be caused by two factors – i.e. the attenuation due to the lossy dielectric material $a_{z(d)}$, and that due to the ohmic losses in imperfectly conducting walls $a_{z(c)}$ (Cheng, 1989)

$$a_z = a_{z(d)} + a_{z(c)} , \tag{14}$$

For a conducting waveguide, the inner core is usually filled with low-loss dielectric material, such as air. Hence, $a_{z(d)}$ in (14) shall be assumed zero in the power-loss method and the loss in a waveguide is assumed to be caused solely by the conduction loss. It could be seen later that such assumption is not necessary in the new boundary-matching method. Indeed, the new method inherently accounts for both kinds of losses in its formulation.

The approximate power-loss method assumes that the fields' expression in a highly but imperfectly conducting waveguide, to be the same as those of a lossless waveguide. Hence, k_x, k_y, and k_z are given as (Cheng, 1989)

$$k_x = \frac{m\pi}{a} \tag{15}$$

$$k_y = \frac{n\pi}{b} \tag{16}$$

$$k_z = \beta_z \tag{17}$$

where a and b are the width and height, respectively, of the rectangular waveguide; whereas m and n denote the number of half cycle variations in the x and y directions, respectively. Every combination of m and n defines a possible mode for TE$_{mn}$ and TM$_{mn}$ waves.

Conduction loss is assumed to occur due to small fields' penetration into the conductor surfaces. According to the law of conservation of energy, the attenuation constant due to conduction loss can be derived as (Cheng, 1989)

$$\alpha_z = \frac{P_L}{2P_z} \tag{18}$$

where P_z is the time-average power flowing through the cross-section and P_L the time-average power lost per unit length of the waveguide.

Solving for P_L and P_z based on Poynting's theorem, the attenuation constant a_z for TM and TE modes – i.e. $a_{z(TM)}$ and $a_{z(TE)}$, respectively, can thus be expressed as (Collin, 1991)

$$\alpha_{z(TM)} = \frac{2R_s(m^2b^3 + n^2a^3)}{\eta ab\sqrt{1 - \left(\frac{f_c}{f}\right)^2}\left(m^2b^2 + n^2a^2\right)} \tag{19}$$

$$\alpha_{z(TE)} = \frac{2R_s}{\eta b\sqrt{1 - \left(\frac{f_c}{f}\right)^2}}\left\{\left(1 + \frac{b}{a}\right)\left(\frac{f_c}{f}\right)^2 + \frac{b}{a}\left[1 - \left(\frac{f_c}{f}\right)^2\right]\left[\frac{m^2ab + n^2a^2}{(mb)^2 + (na)^2}\right]\right\} \tag{20}$$

where R_s is the surface resistance, f_c the cutoff frequency, and η the intrinsic impedance of free space.

6. The new boundary-matching method

It is apparent that, in order to derive the approximate power-loss equations illustrated in section 5, the field equations must be assumed to be lossless. In a lossless waveguide, the boundary condition requires that the resultant tangential electric field E_t and the normal derivative of the tangential magnetic field $\partial H_t/\partial a_n$ to vanish at the waveguide wall, where a_n is the normal direction to the waveguide wall. In reality, however, this is not exactly the case. The conductivity of a practical waveguide is finite. Hence, both E_t and $\partial H_t/\partial a_n$ are not exactly zero at the boundary of the waveguide. Besides, the loss tangent of a material decreases in direct proportion with the increase of frequency. Hence, a highly conducting wall at low frequency may exhibit the properties of a lossy dielectric at high frequency, resulting in inaccuracy using the assumption at millimeter and submillimeter wavelengths.

In order to model the field expressions closer to those in a lossy waveguide and to account for the presence of fields inside the walls, two phase parameters have been introduced in the new method. The phase parameters – i.e ϕ_x and ϕ_y, are referred to as the field's penetration factors in the x and y directions, respectively. It is worthwhile noting that, with the introduction of the penetration factors, E_t and $\partial H_t/\partial a_n$ do not necessarily decay to zero at the boundary, therefore allowing the effect of not being a perfect conductor at the waveguide wall.

6.1 Fields in a lossy rectangular waveguide

For waves propagating in a lossy hollow rectangular waveguide, as shown in Figure 3, a superposition of TM and TE waves is necessary to satisfy the boundary condition at the wall (Stratton, 1941; Yassin et al., 2003). The longitudinal electric and magnetic field components E_z and H_z, respectively, can be derived by solving Helmholtz's homogeneous equation in

Cartesian coordinate. Using the method of separation of variables (Cheng, 1989), the following set of field equations is obtained

$$E_z = E_0 \sin\left(k_x x + \phi_x\right)\sin\left(k_y y + \phi_y\right)$$ (21)

$$H_z = H_0 \cos\left(k_x x + \phi_x\right)\cos\left(k_y y + \phi_y\right)$$ (22)

where E_0 and H_0 are constant amplitudes of the fields.

The propagation constant k_z for each mode will be found by solving for k_x and k_y and substituting the results into the dispersion relation

$$k_z = \sqrt{k_0^2 - k_x^2 - k_y^2}$$ (23)

Equations (21) and (22) must also apply to a perfectly conducting waveguide. In that case E_z and $\partial H_z / \partial a_n$ are either at their maximum magnitude or zero at both $x = a/2$ and $y = b/2$ – i.e. the centre of the waveguide, therefore

$$\sin\left(\frac{k_x a}{2} + \phi_x\right) = \sin\left(\frac{k_y b}{2} + \phi_y\right) = \pm 1 \text{ or } 0$$ (24)

Solving (24), the penetration factors are obtained as,

$$\phi_x = \frac{\left(m\pi - k_x a\right)}{2}$$ (25)

$$\phi_y = \frac{\left(n\pi - k_y b\right)}{2}$$ (26)

For waveguides with perfectly conducting wall, $k_x = m\pi/a$ and $k_y = n\pi/b$, (25) and (26) result in zero penetration and E_z and H_z in (21) and (22) are reduced to the fields of a lossless waveguide. To take the finite conductivity into account, k_x and k_y are allowed to take complex values yielding non-zero penetration of the fields into the waveguide material

$$k_x = \beta_x - j\alpha_x$$ (27)

$$k_y = \beta_y - j\alpha_y$$ (28)

where β_x and β_y are the phase constants and a_x and a_y are the attenuation constants in the x and y directions, respectively. Substituting the transverse wavenumbers in (27) and (28) into (23), the propagation constant of the waveguide k_z results in a complex value, therefore, yielding loss in wave propagation.

Substituting (21) and (22) into (10) to (13), the fields are obtained as

$$H_x = \frac{j\left[k_z k_x H_0 + \omega\varepsilon_0 k_y E_0\right]\sin(k_x x + \varphi_x)\cos(k_y y + \phi_y)}{k_x^2 + k_y^2}$$ (29)

$$H_y = \frac{j\left[k_z k_y H_0 - \omega\varepsilon_0 k_x E_0\right]\cos(k_x x + \phi_x)\sin(k_y y + \phi_y)}{k_x{}^2 + k_y{}^2} \tag{30}$$

$$E_x = -\frac{j\left[k_z k_x E_0 - \omega\mu_0 k_y H_0\right]\cos(k_x x + \phi_x)\sin(k_y y + \phi_y)}{k_x{}^2 + k_y{}^2} \tag{31}$$

$$E_y = -\frac{j\left[k_z k_y E_0 + \omega\mu_0 k_x H_0\right]\sin(k_x x + \phi_x)\cos(k_y y + \phi_y)}{k_x{}^2 + k_y{}^2} \tag{32}$$

where μ_0 and ε_0 are the permeability and permittivity of free space, respectively.

6.2 Formulation

At the wall, the tangential fields must satisfy the relationship defined by the constitutive properties μ_c and ε_c of the material. The ratio of the tangential component of the electric field to the surface current density at the conductor surface is represented by (Yeap et al., 2009b; Yeap et al., 2010)

$$\frac{E_t}{a_n \times H_t} = \sqrt{\frac{\mu_c}{\varepsilon_c}} \tag{33}$$

where μ_c and ε_c are the permeability and permittivity of the wall material, respectively, and $\sqrt{\dfrac{\mu_c}{\varepsilon_c}}$ is the intrinsic impedance of the wall material. The dielectric constant is complex and ε_c may be written as

$$\varepsilon_c = \varepsilon_0 - j\frac{\sigma_c}{\omega} \tag{34}$$

where σ_c is the conductivity of the wall.

In order to estimate the loss of waves in millimeter and submillimeter wavelengths more accurately, a more evolved model than the conventional constant conductivity model used at microwave frequencies is necessary. Here, Drude's model is applied for the frequency dependent conductivity σ_c (Booker, 1982)

$$\sigma_c = \frac{\sigma}{(1 + j\omega\tau)} \tag{35}$$

where σ is the conventional constant conductivity of the wall material and τ the mean free time. For most conductors, such as Copper, the mean free time τ is in the range of 10^{-13} to 10^{-14} s (Kittel, 1986).

At the width surface of the waveguide, $y = b$, $E_z/H_x = -E_x/H_z = \sqrt{\dfrac{\mu_c}{\varepsilon_c}}$. Substituting (21), (22), (29), and (31) into (33), the following relationships are obtained

$$\frac{-E_x}{H_z} = \frac{j}{k_x{}^2 + k_y{}^2}\left(\frac{E_0}{H_0}k_z k_x - \omega\mu_0 k_y\right)\tan\left(k_y b + \phi_y\right) = \sqrt{\frac{\mu_c}{\varepsilon_c}} \tag{36a}$$

$$\frac{H_x}{E_z} = \frac{j}{k_x{}^2 + k_y{}^2}\left(\frac{H_0}{E_0}k_z k_x + \omega\varepsilon_0 k_y\right)\cot\left(k_y b + \phi_y\right) = \sqrt{\frac{\varepsilon_c}{\mu_c}} \tag{36b}$$

Similarly, at the height surface where $x = a$, we obtain $E_y/H_z = -E_z/H_y = \sqrt{\dfrac{\mu_c}{\varepsilon_c}}$. Substituting (21), (22), (30), and (32) into (33), the following relationships are obtained

$$\frac{E_y}{H_z} = \frac{-j}{k_x{}^2 + k_y{}^2}\left(\frac{E_0}{H_0}k_z k_y + \omega\mu_0 k_x\right)\tan\left(k_x a + \phi_x\right) = \sqrt{\frac{\mu_c}{\varepsilon_c}} \tag{37a}$$

$$\frac{-H_y}{E_z} = \frac{-j}{k_x{}^2 + k_y{}^2}\left(\frac{H_0}{E_0}k_z k_y - \omega\varepsilon_0 k_x\right)\cot\left(k_x a + \phi_x\right) = \sqrt{\frac{\varepsilon_c}{\mu_c}} \tag{37b}$$

In order to obtain nontrivial solutions for (36) and (37), the determinant of the equations must be zero (Yeap et al., 2009a). By letting the determinant of the coefficients of E_0 and H_0 in (36) and (37) vanish the following transcendental equations are obtained

$$\left[\frac{j\omega\mu_0 k_y \tan\left(k_y b + \phi_y\right)}{k_x{}^2 + k_y{}^2} + \sqrt{\frac{\mu_c}{\varepsilon_c}}\right]\left[\frac{j\omega\varepsilon_0 k_y \cot\left(k_y b + \phi_y\right)}{k_x{}^2 + k_y{}^2} - \sqrt{\frac{\varepsilon_c}{\mu_c}}\right] = \left[\frac{k_z k_x}{k_x{}^2 + k_y{}^2}\right]^2 \tag{38a}$$

$$\left[\frac{j\omega\mu_0 k_x \tan\left(k_x a + \phi_x\right)}{k_x{}^2 + k_y{}^2} + \sqrt{\frac{\mu_c}{\varepsilon_c}}\right]\left[\frac{j\omega\varepsilon_0 k_x \cot\left(k_x a + \phi_x\right)}{k_x{}^2 + k_y{}^2} - \sqrt{\frac{\varepsilon_c}{\mu_c}}\right] = \left[\frac{k_z k_y}{k_x{}^2 + k_y{}^2}\right]^2 \tag{38b}$$

Since the dominant TE_{10} mode has the lowest cutoff frequency among all modes and is the only possible mode propagating alone, it is of engineering importance. In the subsequent sections, comparison and detail analysis of the TE_{10} mode shall be performed. For the TE_{10} mode, m and n are set to 1 and 0, respectively. Substituting $m = 1$ and $n = 0$ into the penetration factors in (25) and (26), the transcendental equations in (38) for TE_{10} mode can be simplified to

$$\left[\sqrt{\frac{\mu_c}{\varepsilon_c}} + \frac{j\omega\mu_0 k_y \tan\left(k_y \frac{b}{2}\right)}{k_x{}^2 + k_y{}^2}\right]\left[\sqrt{\frac{\varepsilon_c}{\mu_c}} - \frac{j\omega\varepsilon_0 k_y \cot\left(k_y \frac{b}{2}\right)}{k_x{}^2 + k_y{}^2}\right] = \left[\frac{jk_z k_x}{k_x{}^2 + k_y{}^2}\right]^2 \tag{39a}$$

$$\left[\sqrt{\frac{\mu_c}{\varepsilon_c}} - \frac{j\omega\mu_0 k_x \cot\left(k_x \frac{a}{2}\right)}{k_x{}^2 + k_y{}^2}\right]\left[\sqrt{\frac{\varepsilon_c}{\mu_c}} + \frac{j\omega\varepsilon_0 k_x \tan\left(k_x \frac{a}{2}\right)}{k_x{}^2 + k_y{}^2}\right] = \left[\frac{jk_z k_y}{k_x{}^2 + k_y{}^2}\right]^2 \tag{39b}$$

In the above equations, k_x and k_y are the unknowns and k_z can then be obtained from the dispersion relation in (23). A multi root searching algorithm, such as the Powell Hybrid root searching algorithm in a NAG routine, can be used to find the roots of k_x and k_y. The routine requires initial guesses of k_x and k_y for the search. For good conductors, suitable guess values are clearly those close to the perfect conductor values i.e. $\beta_x = m\pi/a$, $\beta_y = n\pi/b$, $a_x = a_y = 0$. Hence, for the TE$_{10}$ mode, the initial guesses for k_x and k_y are π/a and 0 respectively.)

6.3 Experimental setup

To validate the results, experimental measurements had been carried out. The loss as a function of frequency for a rectangular waveguide was measured using a Vector Network Analyzer (VNA). A 20 cm copper rectangular waveguide with dimensions of a = 1.30 cm and b = 0.64 cm such as that shown in Fig. 4 were used in the measurement.

To minimize noise in the waveguide, a pair of chokes had also been designed and fabricated as shown in Fig. 5. A detail design of the choke drawn using AutoCAD are shown in Fig. 6(a) and Fig. 6(b).

In order to allow the waveguide to be connected to the adapters which are of different sizes, a pair of taper transitions had also been used as shown in Fig. 7. Fig. 8 depicts the complete setup of the experiment where the rectangular waveguide was connected to the VNA via tapers, chokes, coaxial cables, and adapters. Before measurement was carried out, the coaxial cables and waveguide adapters were calibrated to eliminate noise from the two devices. The loss in the waveguide was then observed from the S$_{21}$ or S$_{12}$ parameter of the scattering matrix. The measurement was performed in the frequencies at the vicinity of cutoff.

Fig. 4. Rectangular waveguides with width a = 1.30 cm and height b = 0.64 cm.
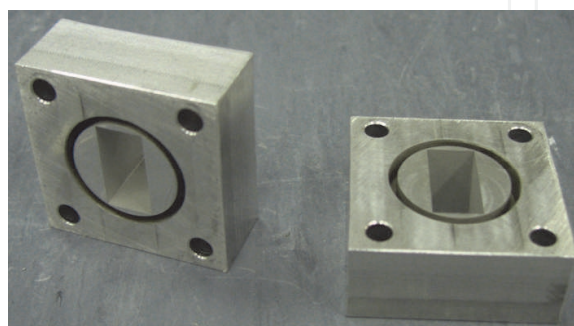

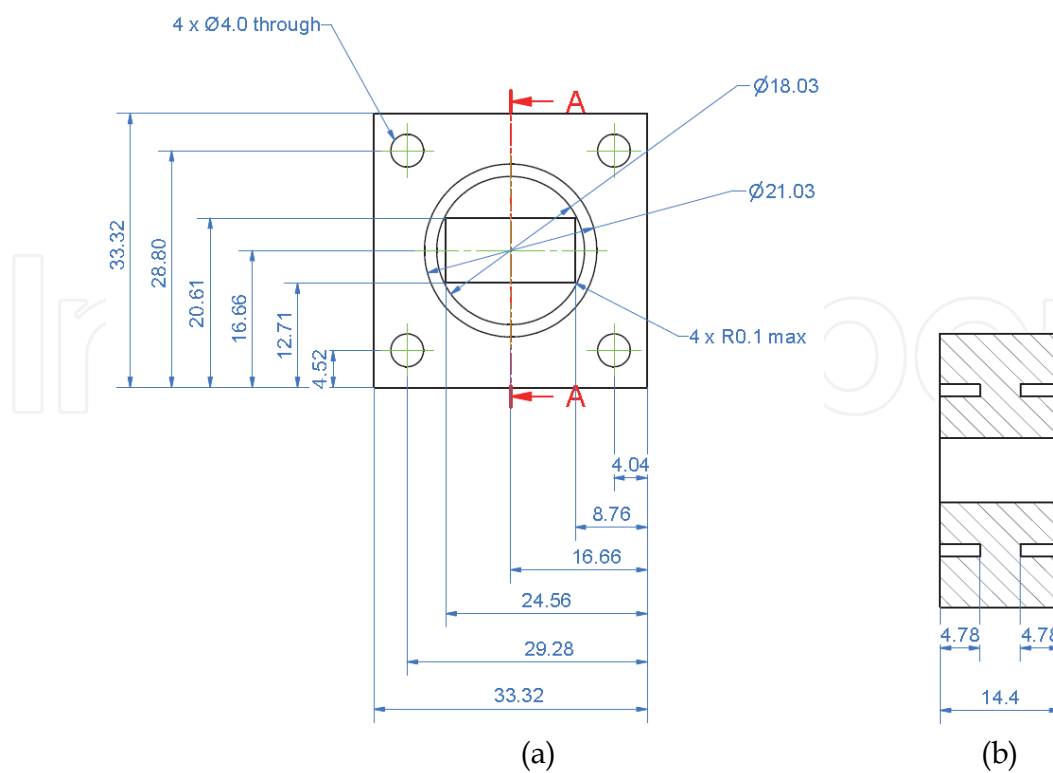Fig. 5. A pair of chokes made of aluminum.

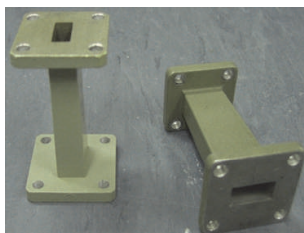Fig. 6. Parameters of the (a) cross section and (b) side view of the choke.
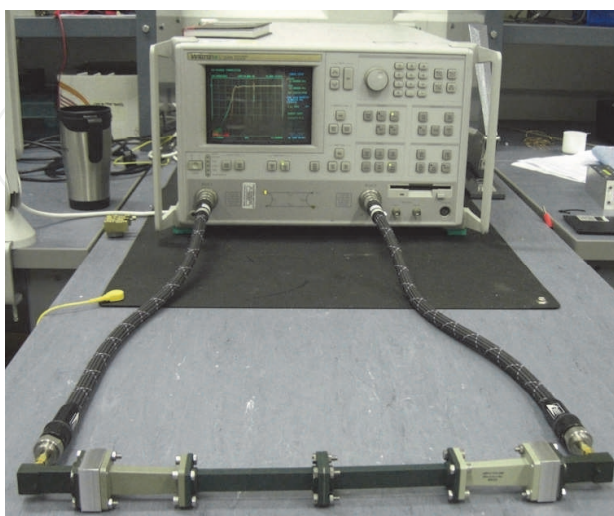

Fig. 7. Taper transitions.

Fig. 8. A 20 cm rectangular waveguide connected to the VNA, via tapers, chokes, adapters, and coaxial cables.

6.4 Results and discussion

As shown in Fig. 9, a comparison among the attenuation of the TE_{10} mode near cutoff as computed by the new method, the conventional power-loss method, and the measured S_{21} result was performed. Clearly, the attenuation constant a_z computed from the power-loss method diverges sharply to infinity, as the frequency approaches f_c, and is very different to the simulated results, which show clearly that the loss at frequencies below f_c is high but finite. The attenuation computed using the new boundary-matching method, on the other hand, matches very closely with the S_{21} curve, measured using from the VNA. As shown in Table 2, the loss between 11.47025 GHz and 11.49950 GHz computed by the boundary-matching method agrees with measurement to within 5% which is comparable to the error in the measurement. The inaccuracy in the power-loss method is due to the fact that the fields expressions are assumed to be lossless – i.e. k_x and k_y are taken as real variables. Analyzing the dispersion relation in (23), it could be seen that, in order to obtain a_z, k_x and/or k_y must be complex, given that the wavenumber in free space is purely real. Although the initial guesses for k_x and k_y applied in the new boundary-matching method are assumed to be identical with the lossless case, the final results actually converge to complex values when the characteristic equations are solved numerically.
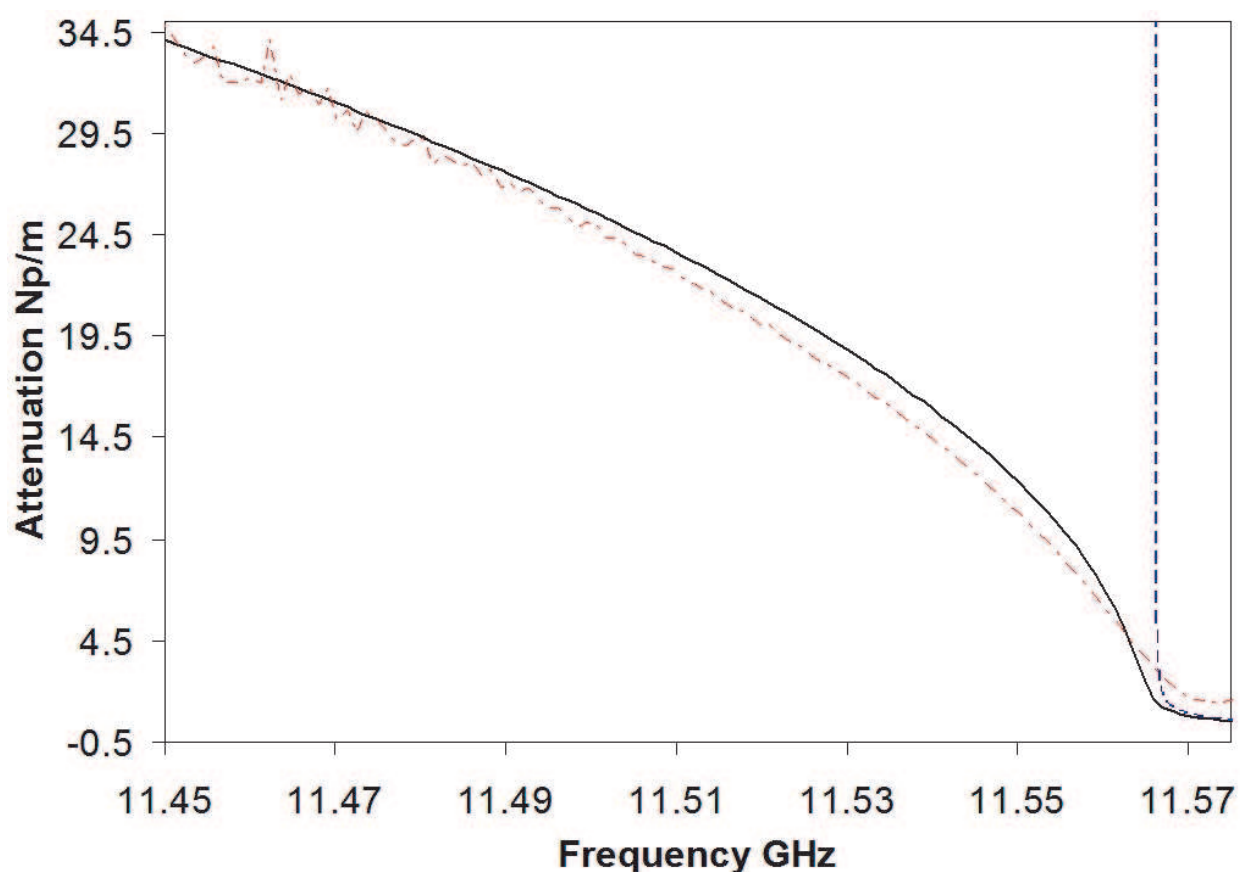

Fig. 9. Attenuation of TE_{10} mode at the vicinity of cutoff. ——————— the new boundary matching method. - - - - - - - - - - power loss method. -·-··-··-··-··- S21 measurement.

Fig. 10 shows the attenuation curve when the frequency is extended to higher values. Here, the loss due to TE_{10} alone could no longer be measured alone, since higher-order modes, such as TE_{11} and TM_{11}, etc., start to propagate. Close inspection shows that the loss

predicted by the two methods at higher frequencies is in very close agreement. It is, therefore, sufficed to say that, although the power-loss method fails to predict the attenuation near f_c accurately, it is still considered adequate in computing the attenuation of TE_{10} in lossy waveguides, provided that the frequency f is reasonably above the cutoff f_c.

As depicted in Fig. 11, at frequencies beyond millimeter wavelengths, however, the loss computed by the boundary-matching method appears to be much higher than those by the power-loss method. The differences can be attributed to the fact that at extremely high frequencies, the loss tangent of the wall material decreases and the field in a lossy waveguide can no longer be approximated to those derived from a perfectly conducting waveguide. At such high frequencies, the wave propagating in the waveguide is a hybrid mode and the presence of the longitudinal electric field E_z can no longer be neglected.

Frequency GHz	Experiment	Boundary-matching method	%Δ
11.47025	30.17693	30.95782	2.59
11.47138	30.68101	30.77417	0.30
11.47250	29.53345	30.5894	3.58
11.47363	30.51672	30.40349	0.37
11.47475	30.16449	30.21642	0.17
11.47588	29.68032	30.02816	1.17
11.47700	29.09721	29.8387	2.55
11.47813	28.85077	29.648	2.76
11.47925	29.25528	29.45606	0.69
11.48038	29.20923	29.26283	0.18
11.48150	27.99881	29.06831	3.82
11.48263	28.38341	28.87245	1.72
11.48375	28.18551	28.67524	1.74
11.48488	27.91169	28.47664	2.02
11.48600	28.08407	28.27663	0.69
11.48713	27.44495	28.07517	2.30
11.48825	27.67956	27.87224	0.70
11.48938	26.84192	27.66779	3.08
11.49050	26.95767	27.46181	1.87
11.49163	26.60108	27.25425	2.46
11.49275	26.78715	27.04508	0.96
11.49388	26.14928	26.83426	2.62
11.49500	25.83003	26.62174	3.07
11.49613	25.82691	26.4075	2.25
11.49725	25.26994	26.19148	3.65
11.49838	24.82685	25.97365	4.62
11.49950	25.1100	25.75395	2.56

Table 1. Attenuation of TE_{10} at the vicinity of the cutoff frequency.

Unlike the power-loss method which only gives the value of the attenuation constant, one other advantage of the boundary-matching method is that it is able to account for the phase
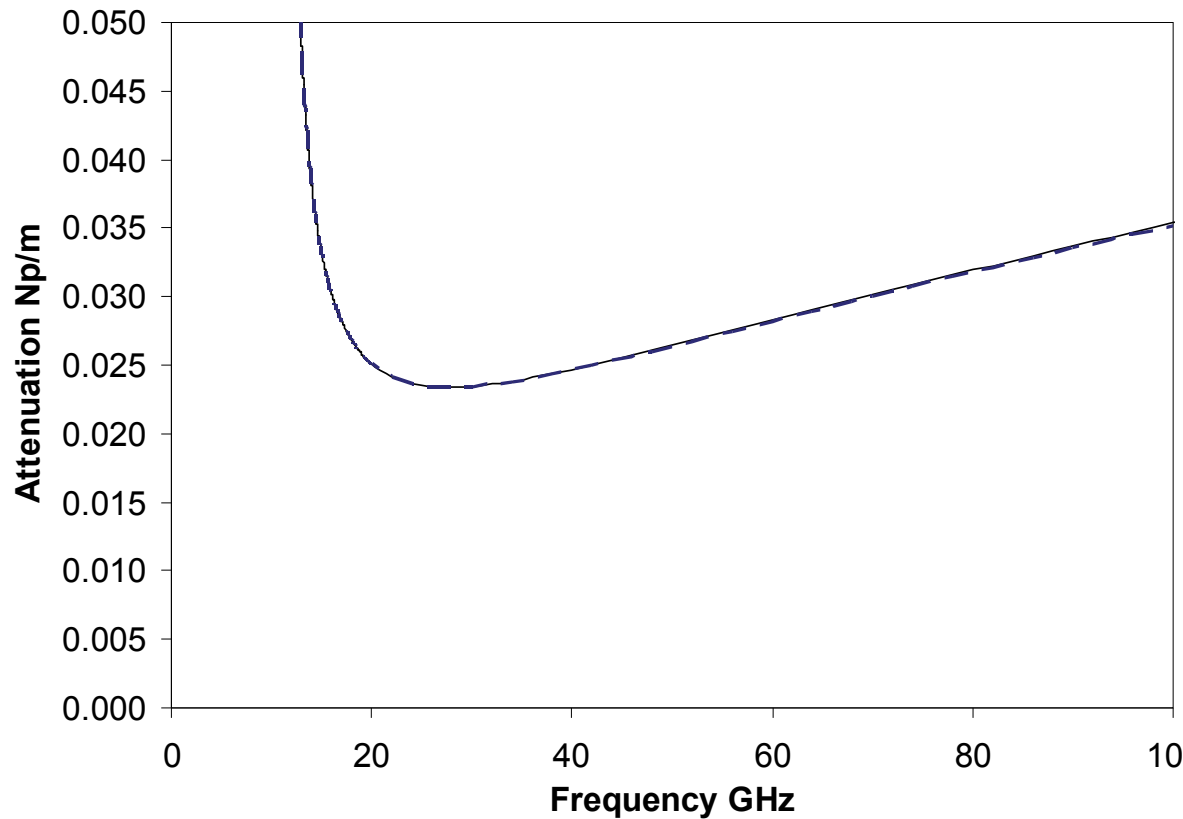
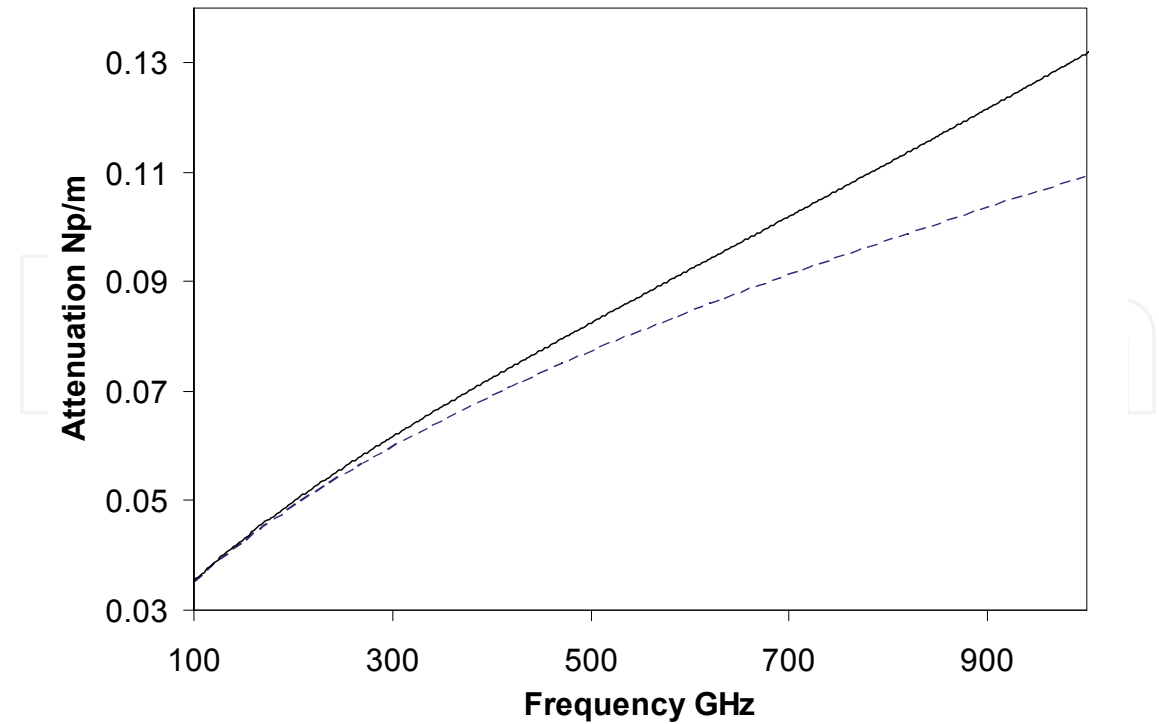Fig. 10. Attenuation of TE_{10} mode from 0 to 100 GHz. ———————— the new boundary matching method. - - - - - - - - - - - power loss method.

Fig. 11. Attenuation of TE_{10} mode from 100 GHz to 1 THz. ——————— the new boundary matching method. - - - - - - - - - - power loss method.

constant of the wave as well. A comparison between the attenuation constant and phase constant of a TE$_{10}$ mode is shown in Fig. 12. As can be observed, as the attenuation in the waveguide gradually decreases, the phase constant increases. Fig. 12 illustrates the change in the mode – i.e. from evanescent below cutoff to propagating mode above cutoff.
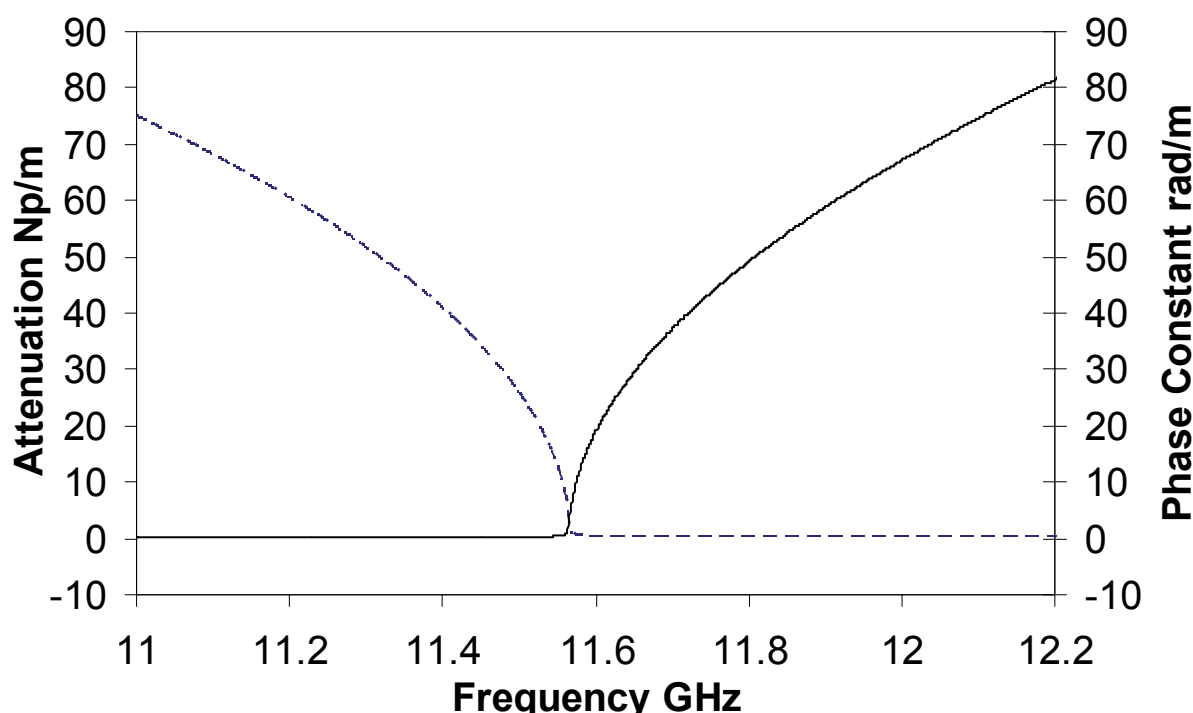

Fig. 12. Propagation constant (phase constant and attenuation constant) of TE10 mode in a lossy rectangular waveguide. ——————— phase constant. - - - - - - - - - - - attenuation constant.

7. Summary

A fundamental and accurate technique to compute the propagation constant of waves in a lossy rectangular waveguide is proposed. The formulation is based on matching the fields to the constitutive properties of the material at the boundary. The electromagnetic fields are used in conjunction of the concept of surface impedance to derive transcendental equations, whose roots give values for the wavenumbers in the x and y directions for different TE or TM modes. The wave propagation constant k_z could then be obtained from k_x, k_y, and k_0 using the dispersion relation.

The new boundary-matching method has been validated by comparing the attenuation of the dominant mode with the S21 measurement, as well as, that obtained from the power-loss method. The attenuation curve plotted using the new method matches with the power-loss method at a reasonable range of frequencies above the cutoff. There are however two regions where both curves are found to differ significantly. At frequencies below the cutoff f_c, the power-loss method diverges to infinity with a singularity at frequency $f = f_c$. The new method, however, shows that the signal increases to a highly attenuating mode as the frequencies drop below f_c. Indeed, such result agrees very closely with the measurement result, therefore, verifying the validity of the new method. At frequencies above 100 GHz, the attenuation obtained using the new method increases beyond that predicted by the power-loss method. At f above the millimeter wavelengths, the field in a lossy waveguide

can no longer be approximated to those of the lossless case. The additional loss predicted by the new boundary-matching method is attributed to the presence of the longitudinal E_z component in hybrid modes.

8. Acknowledgment

9. References

Boifot, A. M.; Lier, E. & Schaug-Petersen, T. (1990). Simple and broadband orthomode transducer, *Proceedings of IEE*, 137, pp. 396 – 400

Booker, H. (1982). *Energy in Electromagnetism*. 1st Edition. Peter Peregrinus.

Carter, M. C.; Baryshev, A.; Harman, M.; Lazareff, B.; Lamb, J.; Navarro, S.; John, D.; Fontana, A. -L.; Ediss, G.; Tham, C. Y.; Withington, S.; Tercero, F.; Nesti, R.; Tan, G. -H.; Sekimoto, Y.; Matsunaga, M.; Ogawa, H. & Claude, S. (2004). ALMA front-end optics. *Proceedings of the Society of Photo Optical Instrumentation Engineers*, 5489, pp. 1074 – 1084.

Chattopadhyay, G.; Schlecht, E.; Maiwald, F.; Dengler, R. J.; Pearson, J. C. & Mehdi, I. (2002). Frequency multiplier response to spurious signals and its effects on local oscillator systems in millimeter and submillimeter wavelengths. *Proceedings of the Society of Photo-Optical Instrumentation Engineers*, 4855, pp. 480 – 488.

Cheng, D. K. (1989). *Field and Wave Electromagnetics*, Addison Wesley, ISBN 0201528207, US.

Chou, R. C. & Lee, S. W. (1988). Modal attenuation in multilayered coated waveguides. *IEEE Transactions on Microwave Theory and Techniques*, 36, pp. 1167 – 1176.

Claricoats, P. J. B. (1960a). Propagation along unbounded and bounded dielectric rods: Part 1. Propagation along an unbounded dielectric rod. *IEE Monograph*, 409E, pp. 170 – 176.

Claricoats, P. J. B. (1960b). Propagation along unbounded and bounded dielectric rods: Part 2. Propagation along a dielectric rod contained in a circular waveguide. *IEE Monograph*, 409E, pp. 177 – 185.

Collin, R. E. (1991). *Field Theory of Guided Waves*, John Wiley & Sons, ISBN 0879422378, New York.

Glaser, J. I. (1969). Attenuation and guidance of modes on hollow dielectric waveguides. *IEEE Transactions on Microwave Theory and Techniques (Correspondence)*, 17, pp. 173 – 176.

Kittel, C. (1986). *Introduction to Solid State Physics*, John Wiley & Sons, New York.

Ma, J. (1998). TM-properties of HTS's rectangular waveguides with Meissner boundary condition. *International Journal of Infrared and Millimeter Waves*, 19, pp. 399 – 408.

Paine, S.; Papa, D. C.; Leombruno, R. L.; Zhang, X. & Blundell, R. (1994). Beam waveguide and receiver optics for the SMA. *Proceedings of the 5th International Symposium on Space Terahertz Technology*, University of Michigan, Ann Arbor, Michigan.

Seida, O. M. A. (2003). Propagation of electromagnetic waves in a rectangular tunnel. *Applied Mathematics and Computation*, 136, pp. 405 – 413.

Shankar, N. U. (1986). *Application of digital techniques to radio astronomy measurements*, Ph.D. Thesis. Raman Research Institute. Bangalore University.

Stratton, J. A. (1941). *Electromagnetic Theory*, McGraw-Hill, ISBN 070621500, New York.

Vassilev, V. & Belitsky, V. (2001a). A new 3-dB power divider for millimetre-wavelengths. *IEEE Microwave and Wireless Components Letters*, 11, pp. 30 – 32.

Vassilev, V. & Belitsky, V. (2001b). Design of sideband separation SIS mixer for 3 mm band. *Proceedings of the 12th International Symposium on Space Terahertz Technology*, Shelter Island, San Diego, California.

Vassilev, V.; Belitsky, V.; Risacher, C.; Lapkin, I.; Pavolotsky, A. & Sundin, E. (2004). Design and characterization of a sideband separating SIS mixer for 85 – 115 GHz. *Proceedings of the 15th International Symposium on Space Terahertz Technology*, Hotel Northampton, Northampton, Masachusetts.

Walker, C. K.; Kooi, J. W.; Chan, M.; Leduc, H. G.; Schaffer, P. L.; Carlstrom, J. E. & Phillips, T. G. (1992). A low-noise 492 GHz SIS waveguide receiver. *International Journal of Infrared and Millimeter Waves*, 13, pp. 785 – 798.

Wang, Y.; Qiu, Z. A. & Yalamanchili, R. (1994). Meissner model of superconducting rectangular waveguides. *International Journal of Electronics*, 76, pp. 1151 – 1171.

Winters, J. H. & Rose, C. (1991). High-T_c superconductors waveguides: Theory and applications. *IEEE Transactions on Microwave Theory and Techniques*, 39, pp. 617 – 623.

Withington, S. (2003). Terahertz astronomical telescopes and instrumentation. *Philosophical Transactions of the Royal Society of London*, 362, pp. 395 – 402.

Yalamanchili, R., Qiu, Z. A., Wang, Y. (1995). Rectangular waveguides with two conventional and two superconducting walls. *International Journal of Electronics*, 78, pp. 715 – 727.

Yassin, G., Tham, C. Y. & Withington, S. (2003). Propagation in lossy and superconducting cylindrical waveguides. *Proceedings of* the *14th International Symposium on Space Terahertz Technology*, Tucson, Az.

Yeap, K. H., Tham, C. Y., and Yeong, K. C. (2009a). Attenuation of the dominant mode in a lossy rectangular waveguide. *Proceedings of the IEEE 9th Malaysia International Conference on Communications*, KL., Malaysia.

Yeap, K. H., Tham, C. Y., Yeong, K. C. & Lim, E. H. (2010). Full wave analysis of normal and superconducting microstrip transmission lines. *Frequenz Journal of RF-Engineering and Telecommunications*, 64, pp. 59 – 66.

Yeap, K. H., Tham, C. Y., Yeong, K. C. & Yeap, K. H. (2009b). A simple method for calculating attenuation in waveguides. *Frequenz Journal of RF-Engineering and Telecommunications*, 63, pp. 236 – 240.
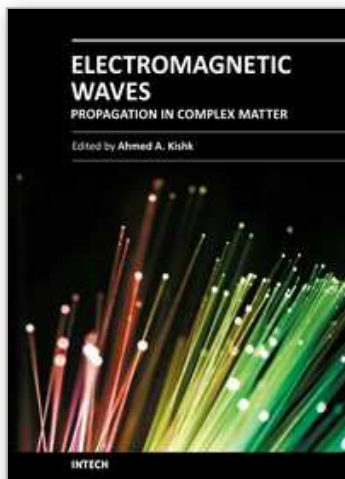
Electromagnetic Waves Propagation in Complex Matter

Edited by Prof. Ahmed Kishk

This volume is based on the contributions of several authors in electromagnetic waves propagations. Several issues are considered. The contents of most of the chapters are highlighting non classic presentation of wave propagation and interaction with matters. This volume bridges the gap between physics and engineering in these issues. Each chapter keeps the author notation that the reader should be aware of as he reads from chapter to the other.

How to reference

In order to correctly reference this scholarly work, feel free to copy and paste the following:

Kim Ho Yeap, Choy Yoong Tham, Ghassan Yassin and Kee Choon Yeong (2011). Propagation in Lossy Rectangular Waveguides, Electromagnetic Waves Propagation in Complex Matter, Prof. Ahmed Kishk (Ed.), ISBN: 978-953-307-445-0, InTech, Available from: http://www.intechopen.com/books/electromagnetic-waves-propagation-in-complex-matter/propagation-in-lossy-rectangular-waveguides1

INTECH
open science | open minds